DOI: 10.1093/jnci/djr290
Advance Access publication on August 10, 2011.

ARTICLE

Role of the Focal Adhesion Protein Kindlin-1 in Breast Cancer Growth and Lung Metastasis

Soraya Sin, Florian Bonin, Valérie Petit, Didier Meseure, François Lallemand, Ivan Bièche, Akeila Bellahcène, Vincent Castronovo, Olivier de Wever, Christian Gespach, Rosette Lidereau, Keltouma Driouch

Manuscript received July 12, 2010; revised July 1, 2011; accepted July 5, 2011.

Correspondence to: Keltouma Driouch, PhD, Institut Curie, Laboratoire d'Oncogénétique, Hôpital René Huguenin, 35 rue Dailly, Saint-Cloud, 92210, France; INSERM, U735, Saint-Cloud, 92210, France (e-mail: keltouma.driouch@curie.net).

Background Fermitin family member 1 (FERMT1, Kindlin-1) is an epithelial-specific regulator of integrin functions and is associated with Kindler syndrome, a genetic disorder characterized by skin blistering, atrophy, and photosensitivity. However, the possible role of kindlin-1 in cancer remains unknown.

Methods Kindlin-1 expression was quantified in several human cancers using quantitative real-time polymerase chain reaction and published microarray datasets. The association between kindlin-1 expression and patient metastasis-free survival (N = 516) was assessed with Kaplan–Meier analyses. Effects of ectopic expression or silencing of kindlin-1 on cell signaling, migration, and invasion were assessed in human breast cancer cell lines using western blotting, immunofluorescence, wound healing assays, and invasion on Matrigel or type I collagen substrates. Breast tumor growth and lung metastasis were evaluated in 12-week-old female BALB/c mice (10 controls and six *Kindlin-1*-knockdown mice). All statistical tests were two-sided.

Results Kindlin-1 expression was consistently higher in tumors than in normal tissues in various cancer types metastasizing to the lungs, including colon and bladder cancer. Kindlin-1 expression was associated with metastasis-free survival in both breast and lung adenocarcinoma (breast cancer: hazard ratio of lung metastasis = 2.55, 95% confidence intervals [CI] = 1.39 to 4.69, $P = .001$; lung cancer: hazard ratio of metastasis = 1.96, 95% CI = 1.25 to 3.07, $P = .001$). Overexpression of kindlin-1 induced changes indicating epithelial–mesenchymal transition and transforming growth factor beta (TGFβ) signaling, constitutive activation of cell motility, and invasion (number of migrating cells, *Kindlin-1* cells vs control, mean = 164.66 vs 19.00, difference = 145.6, 95% CI = 79.1 to 212.2, $P = .004$; invasion rate, *Kindlin-1*-cells vs control = 9.65% vs 1.92%, difference = 7.73%, 95% CI = 4.75 to 10.70, $P < .001$). Finally, Kindlin-1 depletion in an orthotopic mouse model statistically significantly inhibited breast tumor growth ($P < .001$) and lung metastasis ($P = .003$).

Conclusion These results suggest a role for kindlin-1 in breast cancer lung metastasis and lung tumorigenesis and advance our understanding of kindlin-1 as a regulator of TGFβ signaling, offering new avenues for therapeutic intervention against cancer progression.

J Natl Cancer Inst 2011;103:1323–1337

Metastasis, which is responsible for most cancer mortality, occurs through a multistep process, including invasion of tumor cells into the adjacent tissues, intravasation, survival in the circulation, extravasation from blood vessels, initiation and maintenance of micrometastases at distant sites, and finally, growth of cancer cells to produce secondary tumors (1–5). At each step, metastatic cancer cells face multiple obstacles that are overcome with molecular alterations that modify the expression and function of specific metastasis-related genes (1–3,6,7).

Since 2000, the application of genomic profiling methods to the analysis of human breast tumors has generated expression profiles that are predictive of metastasis (8–10). However, although such analyses are very powerful for identifying prognostic markers, it has been difficult to definitively attribute the development of metastasis to the specific contributions of these genes because of the lack of experimental verification. Furthermore, comparative expression profiling of cancer cells with different metastatic potentials in animal models has led to the identification of metastasis promoting genes (8,11–14), although much work remains to be done to validate their clinical relevance. Thus, the characterization of both clinically relevant and functionally important metastasis genes is a crucial step toward the identification of potential therapeutic targets for prevention and treatment.

In previous transcriptomic studies of human metastatic samples (15,16), we identified *Fermitin family member 1* (*FERMT1)*, also called *Kindlin-1*, in a six-gene signature that discriminates primary breast tumors with higher propensity to metastasize to the lungs. Although this signature was suggested to be a surrogate of the

CONTEXTS AND CAVEATS

Prior knowledge

Kindlin-1 encodes one of the three kindlin proteins implicated in several human genetic disorders, including Kindler syndrome, a genetic skin pathology characterized by blistering, atrophy, and photosensitivity. Kindlin-1 may also play a role in several cancers, but the nature of that role is unknown.

Study design

The effects of kindlin-1 overexpression and silencing on cell signaling and metastasis-like functions were assessed in human breast cancer cell lines and in breast tumor growth and lung metastasis in mice. The association between kindlin-1 expression and metastasis-free survival was analyzed in tumor tissue from 516 breast cancer patients.

Contribution

Kindlin-1 expression in human breast tumors was statistically significantly associated with lung metastasis and lung metastasis–free survival. Kindlin-1-expressing cells displayed characteristics that are hallmarks of metastasis, whereas *Kindlin-1*-silencing prevented tumor growth and lung metastasis in mice.

Implications

Kindlin-1 expression may be useful in identifying breast cancer patients with higher risk of developing lung metastasis. In addition, targeting kindlin-1 function may be an effective strategy for blocking metastasis in breast and other cancers.

Limitations

Kindlin-1 expression in other cancers besides breast cancer, which metastasize to the lungs, was not assessed. Although kindlin-1 expression was associated with other genes important in metastasis initiation, the molecular dissection of this association was not addressed.

From the Editors

basal-like subtype of breast cancers, we further demonstrated that it predicts lung metastases independent of the molecular subtypes of breast tumors (16,17).

Kindlin-1 encodes the kindlin-1 protein that belongs to a family of focal adhesion proteins consisting of three members (kindlin-1 to 3). Kindlins have clinical relevance for several human genetic disorders (18–21). In particular, *Kindlin-1* is mutated in Kindler syndrome, a genetic skin pathology characterized by skin blistering, atrophy, and photosensitivity (18,19,22). Kindlins are regulators of integrin signaling and cell-matrix adhesion (23). They were shown to directly bind to β-integrin cytoplasmic tails. This binding, in concert with talin recruitment, leads to the activation (inside-out signaling) of integrins, enabling them to bind to their ligands (20). Following ligand binding, kindlins recruit integrin-linked kinase (ILK) and migfilin to focal adhesion sites (outside-in signaling), thereby linking the extracellular matrix (ECM) to the actin cytoskeleton (24). In line with this adapter function, kindlin-1-deficient cells exhibit defects in β1 integrin activation and impaired cell adhesion, proliferation, polarity, and motility (22,25,26).

Most kindlin-related studies focus on kindlin relevance in skin disease. To date, the biological implications of kindlin-1 have not been shown in cancer. Here, we conducted a study to investigate the role of kindlin-1 at the clinical, cellular, and molecular levels. First, we investigated whether *Kindlin-1* is associated with lung metastasis in human breast cancer and poor prognosis in lung cancer. We then addressed the role of kindlin-1 in the aggressive phenotypes of tumor cells and assessed its involvement in breast cancer progression using an orthotopic mouse model.

Methods

Patients and Cell Lines

Patients. Lung, liver, brain, and bone metastases from breast cancer patients were obtained from the Curie Institute/René Huguenin Hospital (Saint-Cloud, France), the University of L'Aquila (L'Aquila, Italy), and IDIBELL (Barcelona, Spain). In addition, the microarray expression profiles of breast cancer metastases from an independent cohort of patients were analyzed (27).

A total of 516 primary tumors were obtained from the Curie Institute/René Huguenin Hospital. Of those, 502 [66 grade 1, 261 grade 2, and 175 grade 3 tumors, as scored according to Bloom and Richardson histoprognostic grading (28); see Supplementary Table 1, available online] were selected to encompass the various stages of breast cancer progression because grading information was available on those patients. The mean age of the patients was 60.7 years (range = 25–91 years), and the median follow-up was 120.5 months (range = 13–347 months). Seventy-six patients developed lung metastases.

We also analyzed four independent datasets of breast tumors (29–33) and two cohorts of lung cancers (34,35) for which microarray data were publicly available. The breast cancer cohorts "TRANSBIG"(consortium of the Breast International Group, n = 198; http://www.ncbi.nlm.nih.gov/geo/query/acc.cgi?acc=GSE7390), "EMC" (Erasmus Medical Center, n = 344; http://www.ncbi.nlm.nih.gov/geo/query/acc.cgi?acc=GSE2034 and GSE5327), and "NKI" (Netherlands Cancer Institute, n = 295; http://microarray-pubs.stanford.edu/wound_NKI/) consisted of early-stage breast tumors (100%, 100%, and 50% lymph node negative, respectively), whereas the "MSKCC" (Memorial Sloan-Kettering Cancer Center; http://www.ncbi.nlm.nih.gov/geo/query/acc.cgi?acc=GSE2603) cohort (n = 82) consisted of locally advanced tumors (66% lymph node positive).

Paraffin-embedded sections of matching breast tumors and metastases (n = 22) were obtained from the Curie Institute/René Huguenin Hospital and the University of Liège (Belgium). Adjacent normal host tissues were also observed in the same sections.

Written informed consent was obtained from each patient according to the recommendations of the local ethics committee. This study was approved by the review boards and ethics committees of the respective institutions.

Cell Lines. Mouse mammary tumor cell lines 67NR, 168 FARN, 4T07, and 4T1 were kindly provided by Dr Fred Miller (Karmanos Cancer Institute/Wayne State University, Detroit, MI). Human mammary epithelial cells (HMEC) were purchased from Lonza (Walkersville, MA). All other human mammary cell lines HBL-100, MCF7, SK-BR-3, MDA-MB-231, MDA-MB-468, and MDA-MB-435S were purchased from the American Type Culture Collection (ATCC, Manassas, VA). Currently, it is unclear whether MDA-MB-435S is a breast cancer line, because it may

actually be a melanoma line (36). The phenotype of HMEC cells was verified by Lonza by immunostaining for specific markers, and a certificate of analysis confirmed the authentication of cells. The phenotypes of the other cells were verified by ATCC by immunostaining for specific markers. The protocols for verifying the cell lines are available on the ATCC Web site (http://www.atcc.org/Portals/1/Pdf/CellBiologyStandards.pdf). The cell lines 67NR, 168 FARN, and 4T07 were used before passage 20, and the 4T1 cell line was used before passage 13.

All cell lines were maintained at 37°C with 5% CO_2 and grown in Dulbecco's Minimal Essential Medium (DMEM), supplemented with 10% fetal bovine serum (FBS) (Invitrogen, Carlsbad, CA) or 5% FBS [168FARN and 4T1, as previously described (37)] or in Minimal Essential Medium (MCF7) and 1% antibiotics (50 μg/mL penicillin, 50 μg/mL streptomycin, 100 μg/mL neomycin). Transforming growth factor β1 (TGFβ1) and transforming growth factor β receptor 1 (TGFβR1) inhibitor (SB431542) targeting the kinase activity of TGFβR1, were purchased from R&D Systems, Inc (Minneapolis, MN), and Sigma-Aldrich (St Louis, MO), respectively.

Constructs and Transfections

Expression Constructs. The human *Kindlin-1* cDNA, kindly provided by Dr Beckerle (Huntsman Cancer Institute, Salt Lake City, UT), was subcloned into the phCMV2-HA and pIREShyg3 vectors. Transfections were performed using Lipofectamine Reagent (Invitrogen) following the manufacturer's instructions. Stable transfectants were grown in the presence of 1 mg/mL geneticin G418 or 50 μg/mL hygromycin (Sigma-Aldrich). At least two clones of each cell line were used for in vitro experiments to exclude clonal variation.

Luciferase Reporter Assay. For TGFβ-inducible luciferase reporter assays, MDA-MB-231 cells were transfected with the p3TP-lux construct that is a TGFβ1-responsive firefly luciferase reporter gene that contains three consecutive tetradecanoylphorbol acetate (TPA) response elements (TREs) and a portion of the plasminogen activator inhibitor 1 (PAI-1) promoter region (Wrana and Massague, Memorial Sloan-Kettering Cancer Center, New York, NY) (38). For the *E-cadherin* (*CDH1*) promoter luciferase reporter assay, we used pGL3-E-cad(−178/+92) (WT) containing the wild-type *CDH1* promoter or pGL3-E-cad(−178/+92) (MUT) containing the promoter with mutated E-boxes, kindly given by Dr Batlle (ICREA/IRB, Barcelona, Spain) and previously described (39). In all luciferase experiments, cells were cotransfected with pIREShyg3-*Kindlin-1* or pIREShyg3 as control and with pRL-TK (Stratagene, La Jolla, CA), which constitutively expressed Renilla luciferase as an internal standard for the variation of transfection efficiency.

Small Interfering RNA (siRNA)–Mediated RNA Interference. Two different siRNA-coding oligonucleotides against human *Kindlin-1* (Dharmacon, Lafayette, CO) were tested. The *Kindlin-1*-siRNA1–targeting sequence is 5′-CAGCUGCUCUUACGAUUUA-3′ (only sense sequence is shown). The *Kindlin-1*-siRNA2–targeting sequence is 5′-AAACCCAGAUCCUCAGUUA-3′. A non-targeting siRNA oligonucleotide, which did not match any known human coding cDNA, was used as a control (D-001210-03, Dharmacon). Cells were transfected with Hiperfect Reagent (Qiagen, Valencia, CA).

Stable Knockdown. To establish stable silencing of *Kindlin-1*, 4T1 cells were transduced with either *Kindlin-1* short hairpin RNA (shRNA) (two different shRNA were used: SH-041378-01-25 and SH-041378-02-25) or control non-targeting shRNA lentiviral particles (S-005000-01; SMART vector Lentiviral Particules, Dharmacon) using MOI 200 (Multiplicity Of Infection represents the number of transducing lentiviral particles per cell) for 7 hours in six-well plates in the presence of hexadimethrine bromide (5 μg/mL, Sigma-Aldrich). Transduced cells were subjected to selection with 2 μg/mL puromycin (Sigma-Aldrich).

Expression Analyses

Quantitative Real-Time Polymerase Chain Reaction(qRT-PCR). Total RNA extraction, cDNA synthesis, PCR conditions, and normalization methods were described in detail elsewhere (40). Briefly, total RNA was isolated using a standard acid-phenol guanidium method. RNA concentration and purity were measured on the Nanodrop ND-1000 (Nanodrop Technologies, Wilmington, DE). First-strand cDNA was synthesized using a SuperScriptII Reverse Transcriptase kit (Invitrogen) according to the manufacturer's guidelines. All PCR reactions were performed with an ABI Prism 7700 Sequence Detection System (Applied Biosystems, Carlsbad, CA) and the SYBR Green PCR Core Reagents kit (Applied Biosystems). TATA box–binding protein (TBP) transcripts were used as an endogenous RNA control, and each sample was normalized on the basis of its TBP content (40). *Kindlin-1*-specific primers were forward: 5′AAG GAA CTT GAA CAA GGA GAA CCA CT 3′ and reverse: 5′ GGC ACA ACT TCG CAG CCT CTA 3′. For each primer pairs a standard curve was performed using a serial dilution of a pool of cDNAs consisting of several normal tissues (placenta, fetal brain, testis, and breast). The linearity of standard curves was verified, with all coefficients of variation between 0.96 and 0.99.

Antibody Production. Polyclonal antibodies against kindlin-1 were generated by inoculating rabbits with two distinct human kindlin-1 peptides corresponding to amino acids 652–666 (FLSTRSKDQNETLDE) and amino acids 663–677 (TLDEDLFHKLTGGQD) (Eurogentec, Seraing, Belgium). Antibodies were affinity purified on a sepharose matrix.

Immunohistochemistry. Human and murine tumor paraffin sections were prepared as described (15). Briefly, tumor blocks were deparaffinized, treated with 3% H_2O_2, and incubated with rabbit polyclonal anti-kindlin-1 (1:500; Abcam, Cambridge, MA) or rabbit polyclonal anti-E-cadherin (4A2C7 clone, 1:500; Invitrogen). The staining signals were revealed with the Dako Real Detection System, Peroxidase/AEC kit (Dako, Ely, UK). The slides were counterstained with Mayer's hematoxylin.

Western Blotting. Proteins were extracted from cells in culture using TNMG buffer (20 mM Tris–HCl (pH 8), 150 mM NaCl, 5 mM $MgCl_2$, 10% glycerol, 0.5% NP-40, pH 8) supplemented with protease inhibitors. Cell lysates were probed using the

following antibodies: mouse monoclonal anti–α-smooth muscle actin (1A4 clone, 1:500), goat polyclonal anti–β-actin (I-19 clone, 1:200), rabbit polyclonal anti–fibronectin (H-300 clone, 1:1000), goat polyclonal anti–GAPDH (V18 clone, 1:2000), rabbit polyclonal anti–Twist-related protein 1 (H-81 clone, 1:200), and rabbit polyclonal anti–vimentin (S-20 clone, 1:1000) all purchased from Santa Cruz Biotechnology (Santa Cruz, CA); mouse monoclonal anti–E-cadherin (clone 36, 1:5000), mouse monoclonal anti–γ-catenin (15 clone, 1:5000), and mouse monoclonal anti–N-cadherin (clone 32, 1:2500) from BD Biosciences (San Jose, CA); rabbit monoclonal anti–zinc finger protein snail homolog 1 (SNAI1) (C15D3 clone, 1:100), rabbit monoclonal anti–zinc finger protein SNAI2 (C19G7 clone, 1:100), rabbit polyclonal anti–β-catenin (1: 200), rabbit monoclonal anti–phospho-SMAD family homolog (Smad) 2 (S423-425) (clone 25A9, 1:1000), rabbit monoclonal anti–phospho-Smad3 (S465–467) (clone 138D4, 1:1000), and rabbit polyclonal Smad2/3 (1:1000) obtained from Cell Signaling Technology (Danvers, MA). Proteins were detected according to the ECL Western Blotting Analysis System procedure (GE Healthcare, Buckinghamshire, UK). The quantifications were performed using a video camera (Bio-print system; Vilber-Lourmat, Marne la Vallée, France). Optical densitometry was performed using Bio1D software (Vilber-Lourmat).

Cellular Assays

Cell Proliferation. Proliferation of MCF7 transfectants was measured using the MTS (3-(4,5-dimethylthiazol-2-yl)-5-(3-carboxymethoxyphenyl)-2-(4-sulfophenyl)-2H-tetrazolium) assay according to the instructions of the manufacturer (Promega, Madison, WI, USA). The absorbance at 490 nm was performed on a 96-well microplate reader (Dynatech Laboratories MRX, Chantilly, VA).

Clonogenicity Assay. MCF7 transfected cells (1×10^2) were seeded in the presence of 2×10^5 parental cells in 60-mm diameter Petri dishes and maintained for 3 weeks under geneticin selection. Colonies were fixed with methanol and stained with 0.5% crystal violet. Results are representative of three experiments performed in triplicate.

Immunofluorescence. MCF7 and MDA-MB-435S cells were seeded in 24-well plates pre-coated with 5 μg/mL laminin-111, fixed and permeabilized for 10 min with Phosphate Buffered Saline (PBS) containing 4% paraformaldehyde/0.3% triton, and incubated with PBS containing 1.5% bovine serum albumin (BSA). F-actin was localized using fluorescent-labeled phalloidin conjugated to tetramethylrhodamine isothiocyanate (Sigma-Aldrich) at a dilution of 1:100 of a methanolic stock (200 U/mL) solution. Epithelial and mesenchymal markers were labeled with the same antibodies as used for western blots, except for mouse monoclonal anti–ZO-1 antibody (1/ZO-1 clone, 1:5000; BD Biosciences). Cells were then stained with PBS containing 1 μg/ml DAPI (diamidino-2-phenylindole) to visualize the nuclei. Sections were washed in 0.07 M PBS, mounted, and examined with a fluorescence microscope (Eclipse Ti-S Nikon, Melville, NY).

Transwell Migration Assay. Migration assays were performed in triplicate using cell culture inserts with 8.0-μm pore size membranes (Becton Dickinson, Franklin Lakes, NJ) according to the manufacturer's protocol. MCF7 cells (5×10^4) were plated in the top chamber in DMEM. In the bottom chamber, culture medium containing 10% FBS was used as a chemoattractant. For invasion assays, the top chamber was pre-coated with 4 μg/cm^2 of Matrigel (BD Biosciences). Twenty four hours later, cells were fixed, stained using crystal violet, and counted to estimate total membrane area.

Collagen I Invasion Assay. The following precooled components were gently combined and defined as type I collagen solution: four volumes of type I collagen (stock is 3.49 mg/mL), five volumes of calcium- and magnesium-free Hank's balanced salt solution, one volume of MEM (10×), one volume of 0.25M $NaHCO_3$, 2.65 volumes of culture medium, and 0.3 volumes of 1 M NaOH. For each test condition, 1.25 mL of type I collagen solution was added to one well of a six-well plate, homogeneously spread, and solidified on a flat surface in a humidified atmosphere of 10% CO_2 in air at 37°C for at least 1 hour. Control or *Kindlin-1* transfected MCF7 single cells (2×10^5) suspended in 1 mL culture medium were seeded on top of the type I collagen gel and incubated on a flat surface in a humidified atmosphere of 10% CO_2 in air at 37°C. Cell morphology was studied and invasion was scored after 24 hours (41). The number of invasive and noninvasive cells was counted in ten randomly selected microscopic fields of objective 20× using an inverted phase contrast microscope (DMI 3000B; Leica, Wetzlar, Germany). The invasion index was calculated as the ratio of the number of cells that invaded the gel divided by the number of noninvasive cells counted in each field.

Wound Healing Assay. MDA-MB-435S cells were cultured to confluence in 24-well plates pre-coated with 5 μg/mL laminin-111. Monolayers were scratched with a pipette tip and washed with PBS twice to remove debris. Cells were maintained in DMEM with 10% FBS and antibiotics and imaged by phase contrast microscopy (Eclipse TS100, Nikon). Images were captured at the time and 24 hours after scratching.

Transcriptional Reporter Assay. MCF7 and MDA-MB-231 cells (6×10^4) were seeded in 24-well plates for 24 hours. Cells were cotransfected with 0.3 μg of luciferase reporter constructs (p3TP-lux, pGL3-E-cad(−178/+92) WT or pGL3-E-cad(−178/+92) MUT) and 1 μg of pIREShyg3-*Kindlin-1* or pIREShyg3 as a control, and 0.03 μg of pRL-TK Renilla. Two days after transfection, cell extracts were prepared and the luciferase activity was measured using the Dual-Luciferase Reporter Assay System (Promega), following the manufacturer's instructions. Luciferase readings were recorded using a luminometer (Berthold Technologies, Bad Wildbad, Germany). Luciferase activity was normalized to Renilla luciferase activity.

Mouse Studies

All mouse experiments were conducted according to French veterinary guidelines, the Curie Institute guidelines on animal care, and those formulated by the council of Europe for experimental animal use (L358-86/609EEC). Transduced 4T1 cells (5×10^5) were injected subcutaneously into the fourth mammary gland of 12-week-old female BALB/c mice (n = 10 controls and n = 6 *Kindlin-1*-knockdown mice). Twenty-four days later, all mice were killed by cervical dislocation, and primary tumors and lungs were removed,

measured with calipers, and photographed. Tumor volumes were calculated as: volume (cm^3) = $a \times b^2/2$ (a and b are the two registered perpendicular diameters, with $a > b$). Serial lung sections (every 300 μm) were stained with Mayer's hematoxylin. The number of metastatic foci was determined in a blinded manner by two independent anatomopathologists.

Statistical Analysis

All statistical calculations were performed using PASW Statistics (version 18.0; SPSS Inc, Chicago, IL). Comparisons were performed using a two-sided unpaired Student *t* test. All experimental data presented are representative of at least two independent experiments performed in triplicate. To determine whether *Kindlin-1* expression levels were able to define low– and high–lung metastasis risk populations, the optimal cutoff point to categorize patients into the two distinct risk groups was evaluated by use of the receiver operating characteristic method in the training set (n = 516 and 62 for breast and lung cancer, respectively) and then applied to the validation sets (MSKCC, EMC, NKI, or combined cohort for breast cancer and Memorial Sloan-Kettering Cancer Center, Dana-Farber Cancer Institute, or combined cohort for lung cancer). Survival distributions were estimated by the Kaplan–Meier method, and the significance of differences between survival rates was ascertained using the log-rank test. Multivariable analysis using Cox proportional hazards model was used to assess the independent contribution of each variable to lung metastasis–free survival. All variables included in the Cox model were categorical: estrogen receptor status was considered negative or positive according to the anatomopathological examination; lymph node status was referred to as positive when at least one lymph node was affected; the basal-like subtype was evaluated according to the intrinsic gene signature (42), and the "Lung Metastasis Signature" as reported in Minn et al. (12). The proportional hazards assumption was tested using tests and graphs based on the Schoenfeld residuals.

Oncomine database queries (https://www.oncomine.org) were performed using the same criteria for all tested cancer types. Briefly, we searched all of the gene expression datasets for the *Kindlin-1* gene in the "cancer versus normal analysis" category. To avoid discrepancies among the results, we used the same Affymetrix probe (218796_at) Affymetrix, Santa Clara, CA. All studies are presented in the results section, except two out of four datasets on prostate cancer because they all gave similar results.

All statistical tests were two-sided. *P* values less than .05 were considered to be statistically significant, and where appropriate, the difference in means and the 95% confidence interval (95% CI) are indicated.

Results

Evaluation of Kindlin-1 as a Breast Cancer Lung Metastasis–Associated Gene

We previously identified (15) *Kindlin-1* as a highly differentially expressed gene in lung metastases from primary breast tumors compared with metastases in other organs (6.9-fold increase, $P < .001$, Student *t* test). These microarray results have been confirmed both at the mRNA and protein levels in additional samples of metastases (Supplementary Figure 1, A and B, available online). Kindlin-1 expression was visible in lung metastases but not in adjacent host parenchyma (Supplementary Figure 1, B, available online), indicating that kindlin-1 is specifically expressed by cancer cells. Non-lung metastases showed low to no kindlin-1 expression (Supplementary Figure 1, B, available online).

Because kindlin-1 was also detected in primary breast tumors metastasizing to the lungs (15,16), we further investigated whether its expression was associated with breast cancer progression in a series of 198 primary tumors (lymph node–negative systemically untreated patients) (33). Transcript levels increased with the tumor grade (mean normalized mRNA levels: grade 1–2 vs grade 3, 3.37 vs 3.94; difference = 0.57, 95% CI = 0.13 to 1.01, $P = .01$, Figure 1, A) and were higher in lung metastases than in primary tumors (mean normalized mRNA levels: grade 1–2 vs lung metastases, 3.37 vs 5.03, difference = 1.66, 95% CI = 1.00 to 2.31, $P < .001$; grade 3 vs lung metastases, 3.94 vs 5.03, difference = 1.09, 95% CI = 0.12 to 2.05, $P = .02$, Figure 1, A).

Moreover, we analyzed whether kindlin-1 is differentially expressed in breast tumors according to the metastatic site. *Kindlin-1* expression was tested by qRT-PCR on an additional sample of 516 primary breast tumors with a well-documented clinical follow-up (Supplementary Table 1, available online). Higher expression was observed in tumors metastasizing to the lung than in tumors metastasizing to bone (mean normalized mRNA levels: lung-metastasizing tumors vs bone-metastasizing tumors, 1.58 vs 0.69, difference = 0.89, 95% CI = 0.33 to 1.46, $P = .002$, Figure 1, B). Immunohistochemical analysis of primary tumors and subsequent metastases (n = 22) confirmed that patients metastasizing to the lungs had strong immunoreactivity in their primary tumors and their lung metastases, but not in their non-lung metastases (Figure 1, C).

Kindlin-1 as a Prognostic Factor for Breast Cancer Lung Metastasis

To test the prognostic value of *Kindlin-1* expression, we performed a univariate analysis on the same sample of tumors from 516 patients (training set). We defined the stratification cutoff to classify patients into high- and low-*Kindlin-1* groups in the training set and generated Kaplan–Meier plots to illustrate the survival differences among these groups for both the training and validation (n = 721) datasets (Figure 1, D and E and Supplementary Figure 2, A and B). Survival analyses revealed that the risk of lung metastasis was statistically significantly higher for patients with increased *Kindlin-1* mRNA levels (lung metastasis–free survival: training set, hazard ratio [HR] of lung metastasis = 1.85, 95% CI = 1.00 to 3.43, $P = .03$; validation set, HR of lung metastasis = 2.55, 95% CI = 1.39 to 4.69, $P = .001$, log-rank test). In contrast, we found no association between *Kindlin-1* expression and the outcome with regard to overall distant metastasis or specific bone metastasis (Supplementary Figure 2, C–E, available online).

To determine whether *Kindlin-1* is associated with a poor prognosis subtype of breast cancer, we analyzed *Kindlin-1* expression in the NKI cohort that was categorized into five molecular subgroups as defined by the "intrinsic signature" (42). Indeed, the basal subgroup with the worst survival rates had the highest levels of *Kindlin-1* transcripts ($P < .001$, Student *t* test, Supplementary Figure 2, F, available online) indicating that kindlin-1 is a marker

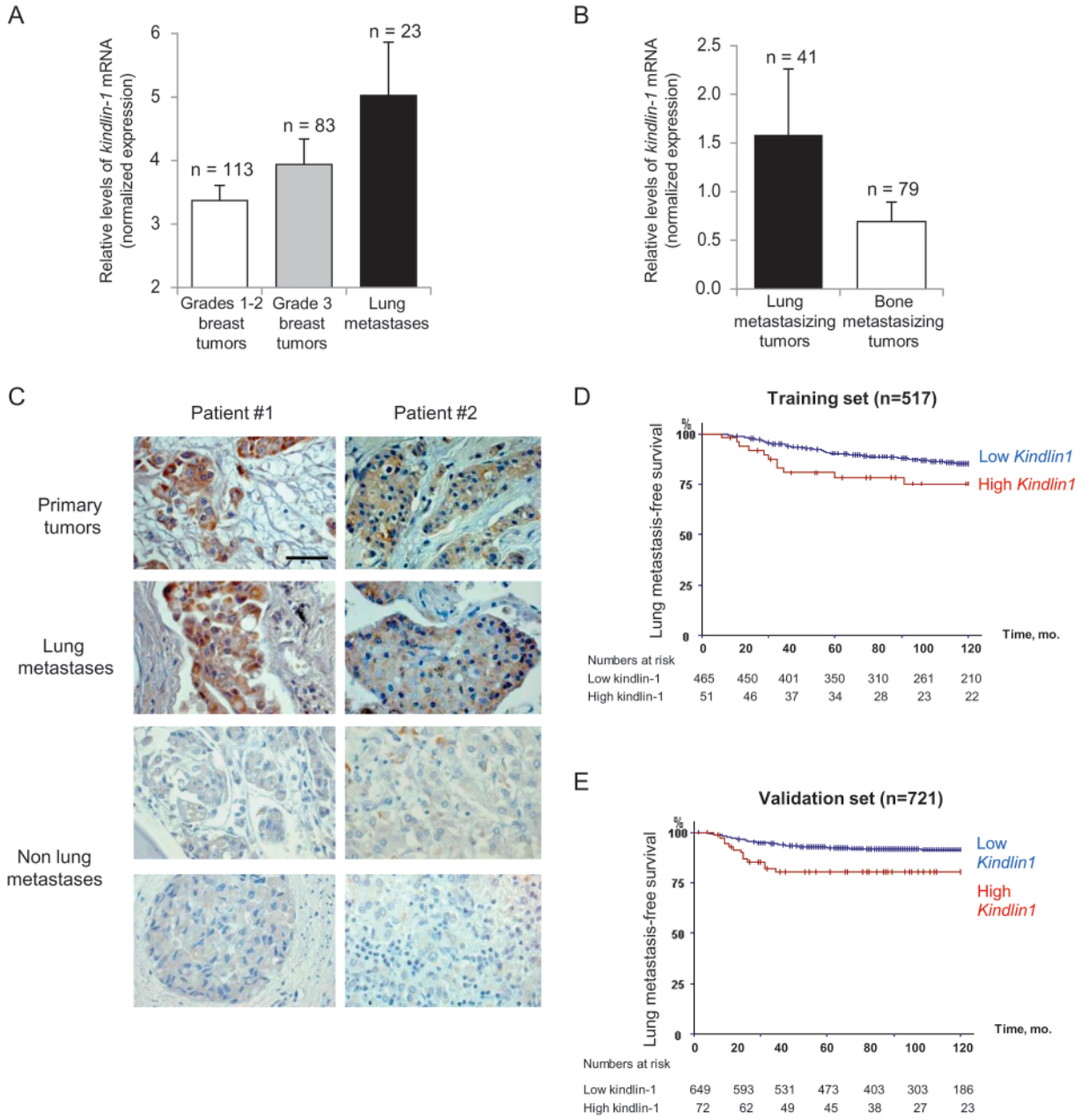

Figure 1. *Kindlin-1* as a prognostic marker for breast cancer lung metastasis. **A**) *Kindlin-1* mRNA expression (relative units) in primary tumors (grades 1–2 or 3; Gene Expression Omnibus accession no. GSE7390) vs lung metastases (GSE11078 and GSE14020) as determined by microarray gene expression. Grades 1–2 vs 3, $P = .01$, grade 3 vs lung metastases, $P = .02$, and grades 1–2 vs lung metastases, $P < .001$, Student *t* test. **B**) *Kindlin-1* expression in tumors metastasizing exclusively to lungs vs to bones, as determined by qRT-PCR on an additional series of 516 primary breast tumors with a well-documented clinical follow-up (Supplementary Table 1, available online). Means and upper 95% CIs are shown for one experiment. $P = .002$, Student *t* test. **C**) Representative immunohistochemical staining of kindlin-1 in matched pairs of primary tumors and metastases from two individuals with breast cancer from a larger sample (n = 22). Non-lung metastases were harvested from the bone (top) and uterus (bottom) of patient 1, and from the liver (top) and spleen (bottom) of patient 2. Original magnification ×400, scale bar = 50 μm. **D**) Kaplan–Meier curves showing the lung metastasis–free survival of patients with tumors expressing high vs low levels of *Kindlin-1* in the training set of 516 breast cancer patients analyzed by qRT-PCR, HR of lung metastasis = 1.85, 95% CI = 1.00 to 3.43, $P = .03$. **E**) Kaplan–Meier curves showing the lung metastasis–free survival of patients with tumors expressing high vs low levels of *Kindlin-1* in the combined cohort of 721 breast cancer patients corresponding to three independent microarray datasets (29–32), HR of lung metastasis = 2.55, 95% CI = 1.39 to 4.69; $P = .001$, log-rank test. All statistical tests were two-sided. CI = confidence interval; HR = hazard ratio; qRT-PCR = quantitative real-time polymerase chain reaction.

of breast tumor aggressiveness and is potentially linked to the basal-like phenotype.

Finally, we performed a multivariable Cox proportional hazards analysis on the validation dataset (n = 721) including the variables *Kindlin-1* expression, estrogen receptor status, lymph node status, basal-like subtype, and the Lung Metastasis Signature derived from a MDA-MB-231 xenograft mouse model (12). *Kindlin-1* expression was the only parameter statistically significantly associated with the risk of breast tumors metastasizing to the lungs (Supplementary Table 2, available online).

Kindlin-1 Expression in Other Types of Epithelial Tumors and Association With the Prognosis of Lung Adenocarcinomas

We analyzed microarray datasets in the Oncomine database to determine whether *Kindlin-1* could be involved in other cancers metastasizing to the lungs. We found that *Kindlin-1* transcripts were consistently higher in tumors than in normal tissues in various cancer types metastasizing to the lungs, including colon cancer (mean normalized mRNA levels in normal vs cancerous tissue: cohort 1, 1.81 vs 2.33, difference = 0.51, 95% CI = 0.44 to 0.59, $P < .001$; cohort 2, 1.99 vs 2.61, difference = −0.62, 95% CI = −0.75 to −0.48, $P < .001$) (43,44) and bladder cancer (mean normalized mRNA levels in normal vs cancerous tissue: cohort 1, −0.27 vs 0.77, difference = 1.04, 95% CI = 0.78 to 1.29, $P < .001$; cohort 2, 1.10 vs 1.53, difference = 0.42, 95% CI = 0.20 to 0.64, $P < .001$) (45,46) (Figure 2, A). In contrast, *Kindlin-1* did not show any overexpression in cancers that do not spread to the lungs such as prostate (mean normalized mRNA levels in normal vs cancerous tissue: cohort 1, 1.45 vs 1.66, difference = 0.21, 95% CI = −0.16 to 0.57, $P = .26$; cohort 2, 0.49 vs 0.54, difference = 0.04, 95% CI = −0.08 to −0.17, $P = .45$) (47,48) and ovarian cancers (mean normalized mRNA levels in normal vs cancerous tissue: cohort 1, −0.02 vs −0.15, difference = 0.13, 95% CI = −0.36 to 0.61, $P = 0.61$; cohort 2, 0.17 vs 1.52, difference = 1.35, 95% CI = 0.37 to 2.32, $P = .01$) (52) (Figure 2, B).

Notably, we also found overexpression of *Kindlin-1* in lung cancers (mean normalized mRNA levels in normal vs cancerous tissue: cohort 1, 0.05 vs 0.51, difference = 0.50, 95% CI = 0.36 to 0.56, $P < .001$; cohort 2, −0.91 vs −0.30, difference = 0.61, 95% CI = 0.36 to 0.87, $P < .001$; cohort 3, 0.08 vs 0.87, difference = 0.79, 95% CI = 0.56 to 1.03, $P < .001$) (49–51) (Figure 2, C). Therefore, we tested whether *Kindlin-1* expression was associated with metastasis-free survival of lung cancer patients. A training set of 62 patients with lung adenocarcinomas (34) were examined for *Kindlin-1* expression. The optimal cutoff to stratify patients into high- and low-*Kindlin-1* groups was determined by use of the receiver operating characteristic method in this cohort of patients and was applied to a validation set of tumors from 166 patients (35). Kaplan–Meier analyses of the validation cohort were used to assess the prognostic value of *Kindlin-1* expression in lung adenocarcinomas and showed that patients expressing high levels of *Kindlin-1* had shorter metastasis-free survival times (metastasis-free survival: training set, HR for metastasis = 3.41, 95% CI = 1.69 to 6.89, $P < .001$; validation set, HR = 1.96, 95% CI = 1.25 to 3.07, $P = .001$, log-rank test, Figure 2, D and Supplementary Figure 3, A–B).

Effect of Kindlin-1 on the Metastatic Capacities of Breast Cancer Cell Lines

Kindlin-1 expression was higher in invasive and metastatic human tumor cell lines (MDA-MB-231 and MDA-MB-468) than in poorly invasive cell lines (MCF7 and SKBR3) (Figure 3, A). Moreover, kindlin-1 was only expressed in the highly metastatic 4T1 cells but not in the three nonmetastatic cell lines (67NR, 168FARN, 4T07), all derived from a single mouse mammary tumor (36). These observations suggest that kindlin-1 increases the metastatic capacities of breast cancer cells. To further investigate this hypothesis, we assessed the effect of stable *Kindlin-1* expression in MCF7 cells on proliferation and clonogenicity. According to the proliferation assay, the number of *Kindlin-1*-cells was 2.7-fold higher than the control cells at 96 hours (Proliferation as measured by optical density at 490 nm for control cells vs *Kindlin-1*-cells, 0.25 vs 0.68, difference = 0.42, 95% CI = 0.34 to 0.51, $P < .001$, Figure 3, B). Moreover, the *Kindlin-1*-cells were more clonogenic than controls. Notably, control cells formed tighter and more compact colonies, whereas the *Kindlin-1* colonies had a dispersed pattern, which may reflect the effects of kindlin-1 on cell spreading, migration, and invasion (Figure 3, C). Indeed, control cells were minimally motile, whereas *Kindlin-1* cells showed statistically significantly more cell migration (number of migrating cells, *Kindlin-1*-cells vs control, 164.66 vs 19.00, difference = 145.6, 95% CI = 79.1 to 212.2, $P = .004$, Figure 3, D). This result was confirmed using a wound healing assay with MDA-MB-435S cancer cells. *Kindlin-1* cells showed a more extensive wound closure area with individual random migratory cell behavior compared with control cells (Figure 3, E). *Kindlin-1*-MCF7 cells were much more invasive through a native collagen-type I matrix (invasion rate, *Kindlin-1* cells vs control = 9.65% vs 1.92%: difference = 7.73%, 95% CI = 4.75% to 10.70%, $P < .001$, Figure 3, F). In addition, *Kindlin-1*-cells showed increased local spreading with formation of cell extensions, whereas control cells had a typical epithelial morphology (Figure 3, G). Moreover, two distinct shRNA showing a similar extinction of *Kindlin-1* expression reduced the migratory and invasive capacities of 4T1 cells (Supplementary Figure 4, A–C).

Implication of Kindlin-1 in the Epithelial–Mesenchymal Transition

We next explored whether *Kindlin-1* overexpression in MCF7 and MDA-MB-435S cells induces morphological changes and cytoskeleton reorganization. Indeed, *Kindlin-1* cells exhibited a disruption in cell contacts, a spindle-shaped and round morphology, and the formation of actin stress fibers and lamellipodia, which are hallmarks of the epithelial–mesenchymal transition (EMT) and cell motility (Figure 4, A). Moreover, *Kindlin-1* cells had increased levels of mesenchymal markers and decreased levels of epithelial markers, consistent with a *Kindlin-1* mediated EMT (Figure 4, B and C). In addition, *Kindlin-1*-MCF7 cells had more diffuse staining of E-cadherin, in contrast to the membrane-localized staining in the control lines (Figure 4, D), suggesting that kindlin-1 overexpression also leads to a redistribution of E-cadherin from the membrane to the cytoplasm.

We used a luciferase reporter assay to examine whether kindlin-1 represses transcription of the E-cadherin gene (*CDH1*). Cells overexpressing *Kindlin-1* had lower *CDH1* promoter activity than control cells (50% decrease in luciferase activity relative to control, difference in fold change: 0.52, 95% CI = 0.43 to 0.60, $P = .001$, Figure 4, E). Mutation of the E-boxes, which are critical for transcriptional repression of *CDH1* (39), abrogated the effect of kindlin-1 on the *CDH1* promoter (Figure 4, E). Moreover, we found that kindlin-1 stimulates the expression of zinc finger protein SNAI2 and Twist-related protein 1, two major *CDH1* repressors (8.5- and 5.4-fold change in relative mRNA levels, respectively), whereas the expression of the zinc finger protein SNAI1 repressor was unaffected (Figure 4, F and data not shown).

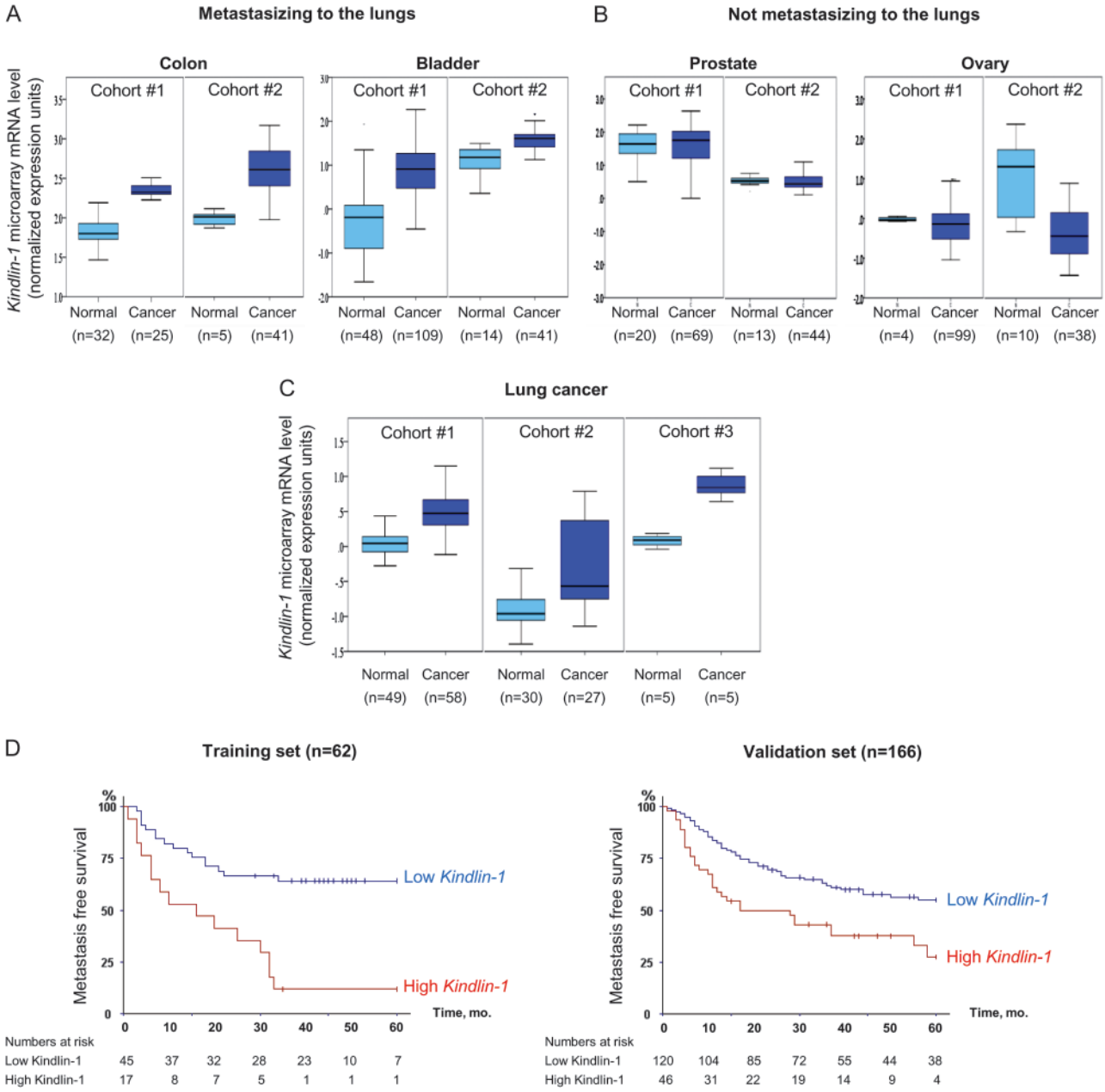

Figure 2. *Kindlin-1* involvement in other cancer types. **A**) *Kindlin-1* expression in tissue from tumors metastasizing to the lungs. **Box plots** of *Kindlin-1* expression levels (normalized expression units) in independent microarray studies obtained from the Oncomine database (https://www.oncomine.org). Differences between normal (**light blue**) and cancerous (**dark blue**) tissues are shown for two colon cancer datasets (cohort 1, $P < .001$; cohort 2, $P < .001$, Student *t* test) (43,44) and two bladder cancer datasets (cohort #1: $P < .001$, and cohort #2: $P < .001$, Student *t* test) (45,46). **B**) *Kindlin-1* expression in tissue from tumors not metastasizing to the lungs. Box plots of *Kindlin-1* expression levels (normalized expression units) in independent microarray studies obtained from the Oncomine database (https://www.oncomine.org). Differences between normal (**light blue**) and cancerous (**dark blue**) tissues are shown for two prostate cancer datasets (cohort 1, $P = .26$; cohort #2, $P = .45$, Student *t* test) (47,48) and two ovarian cancer datasets (cohort 1, $P = .61$; cohort 2, $P = .01$, Student *t* test). **C**) Three lung cancer datasets (cohort 1, $P < .001$; cohort 2, $P < .001$; cohort 3, $P < .001$, Student *t* test) (49–51). **D**) Metastasis-free survival rates of a training set of 62 lung cancer patients (34) with tumors expressing high vs low levels of *Kindlin-1* and an independent validation set consisting of 166 patients with lung adenocarcinomas (metastasis-free survival: training set, HR of metastasis = 3.41, 95% CI = 1.69 to 6.89, $P < .001$; validation set, HR of metastasis = 1.96, 95% CI = 1.25 to 3.07, $P = .001$, log-rank test) (35). All statistical tests were two-sided. CI = confidence interval; HR = hazard ratio.

Kindlin-1 and TGFβ Reciprocal Signaling Crosstalk

Because kindlin-1 expression was induced by TGFβ in normal mammary epithelial cells (HMECs) (25), and TGFβ is a key player in EMT, we analyzed the role of kindlin-1 in TGFβ signaling. We used a luciferase reporter assay to determine if TGFβ-dependent transcription is activated in MDA-BM-231 cells expressing *Kindlin-1* compared with control cells (40% increase in luciferase activity relative to control, difference in fold change: 0.39, 95% CI = 0.06 to 0.73, $P = .03$, Figure 5, A). This activation was confirmed in MCF7 cells expressing *Kindlin-1* showing a robust induction of phosphorylated Smad-2 and Smad-3, two downstream effectors of the canonical TGFβ pathway (Figure 5, B).

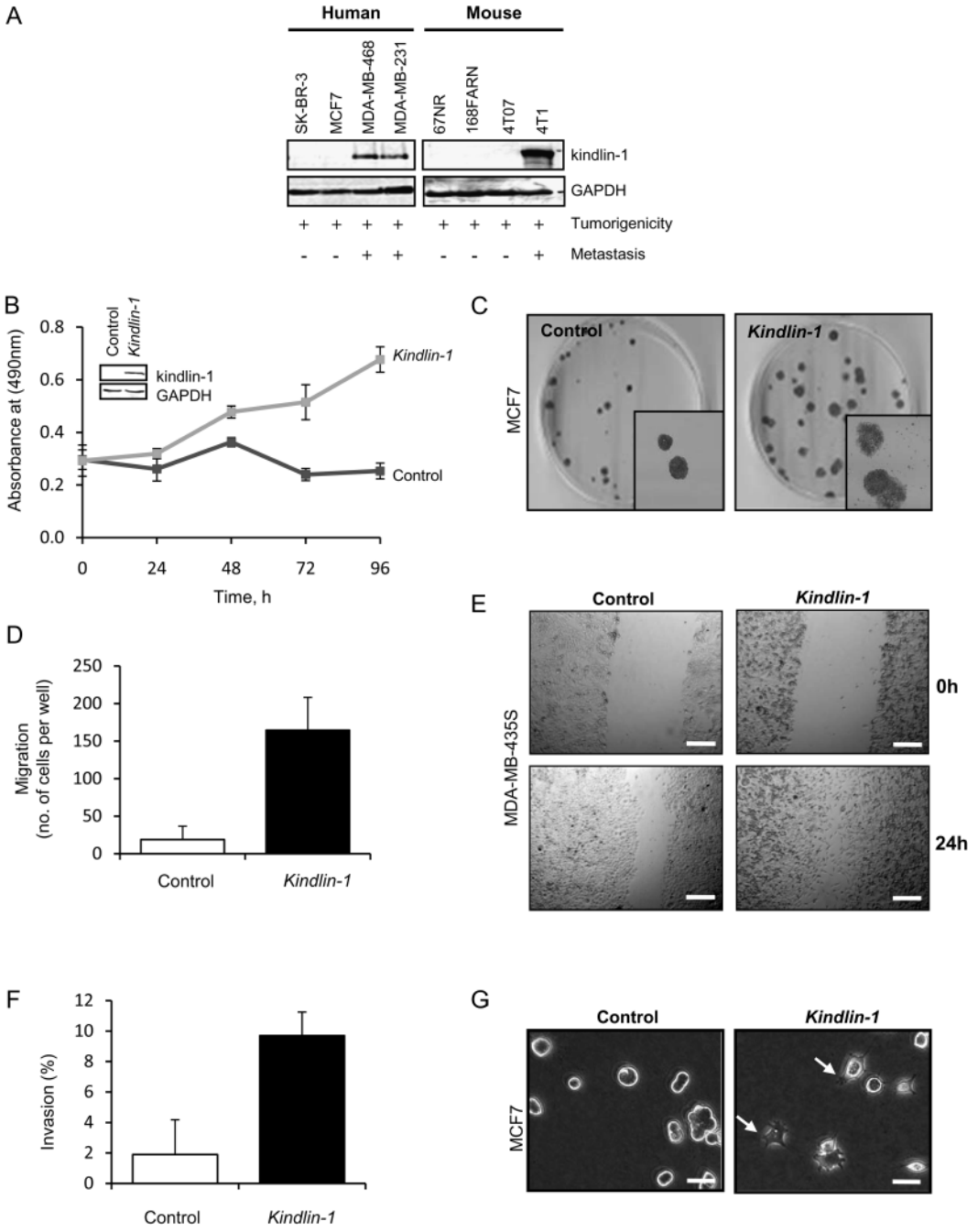

Figure 3. Kindlin-1 involvement in aggressive cancer phenotypes in vitro. **A**) Expression of kindlin-1 protein in human and mouse metastatic and nonmetastatic cell lines. **B**) Effect of ectopic expression of *Kindlin-1* in MCF7 cells on cell proliferation as monitored by the MTS assay. The absorbance at 490 nm was measured at a different time points. Results are representative of three independent experiments performed in triplicate. Means and 95% confidence intervals are shown for one experiment; $P < .001$, Student *t* test. **C**) Clonogenic assays were performed with MCF7 control (left panel) and *Kindlin-1* (right panel) transfectants. The higher magnifications in the insets highlight the morphological differences between colonies of control and *Kindlin-1* cells. **D**) The total number of migrating MCF7 cells was assessed using transwells. Results are representative of two independent experiments performed in triplicate. Means and upper 95% confidence intervals of triplicates are shown for one experiment; $P = .004$, Student *t* test. **E**) Effect of ectopic expression of *Kindlin-1* in MDA-MB-435S cells (right) on a wound healing assay. Microscopic observations were recorded after scratching the cell surface following the indicated periods. Scale bar = 200 μm. **F**) Invasion of MCF7 transfectants was assessed in type I collagen matrix. Results are representative of three independent experiments performed in triplicate. The invasion index was calculated by counting the number of invading and non-invading cells in 10 fields. The means and upper 95% confidence intervals represent one experiment performed in triplicate; $P < .001$, Student *t* test. **G**) Morphology of MCF7 cells in the collagen matrix by phase contrast microscopy. **Arrows** indicate cell extensions. Scale bar = 20 μm. All statistical tests were two-sided.

To confirm the activation of TGFβ signaling, we evaluated the expression levels of several TGFβ target genes that are critical in promoting metastasis (53,54) in *Kindlin-1*-overexpressing MCF7 cells and *Kindlin-1*-depleted HMEC cells. Consistent with our previous results (Figure 5, A and B), the expression of several TGFβ target genes including *connective tissue growth factor* (*CTGF*),

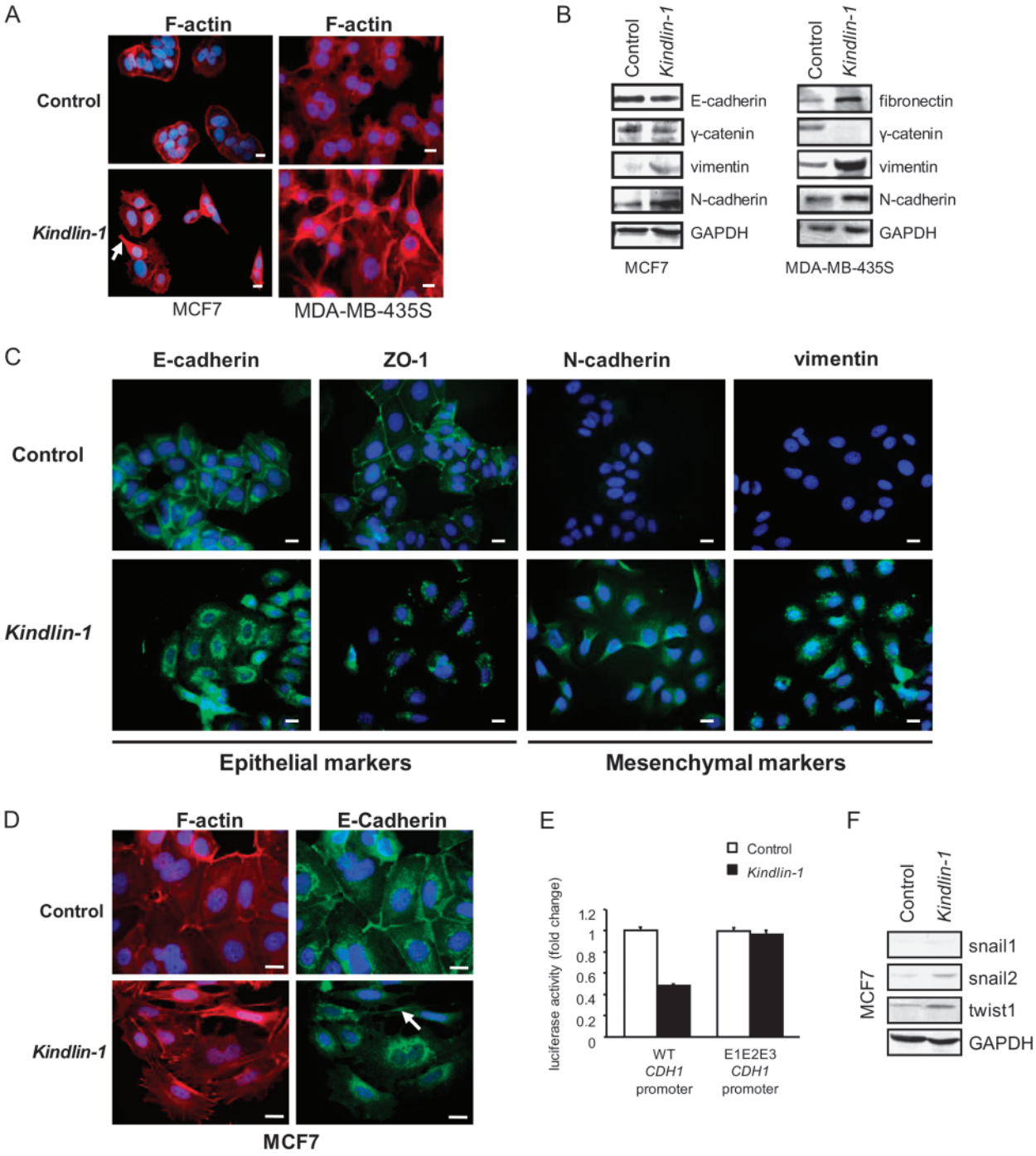

Figure 4. Role of Kindlin-1 in EMT in breast cancer cells. **A**) Morphological changes between control and *Kindlin-1* cells growing on laminin substrate (5 μg/mL) as observed by immunofluorescence microscopy in MCF7 and MDA-MB-435S cells. The cytoskeletal reorganization was visualized by F-actin labeling. The **arrow** shows a lamellipodia-like structure. Scale bar = 20 μm. **B**) Expression of EMT-related proteins (E-cadherin, fibronectin, γ-catenin, vimentin, N-cadherin) in control and *Kindlin-1* cells. **C**) Immunostaining of E-cadherin, ZO-1, N-cadherin, and vimentin in the MCF7 transfectants. Cells were seeded on laminin substrate (5 μg/mL). Cells were then stained with PBS containing 1 μg/mL DAPI (diamidino-2-phenylindole) to visualize the nuclei. Epithelial and mesenchymal markers were labeled with the same antibodies as used for western blots, except for mouse monoclonal anti-ZO-1 antibody (1/ZO-1 clone, 1:5000, BD Biosciences). Scale bar = 20 μm. **D**) Fluorescence staining of F-actin and E-cadherin in the MCF7 transfectants at higher magnification. F-actin was localized using fluorescent-labeled phalloidin conjugated to tetramethylrhodamine isothiocyanate (Sigma-Aldrich) at a dilution of 1:100 of a methanolic stock (200 U/mL) solution. The **arrow** indicates a partial cytoplasmic relocalization of E-cadherin. Scale bar = 20 μm. **E**) MCF7 cells were transfected with the wild-type or mutant pGL3-E-cad reporter construct in the presence or absence of *Kindlin-1*. The luciferase activity was determined and normalized to an internal control. Data are representative of two independent experiments performed in triplicate. Means and upper 95% confidence intervals are shown for triplicates of one experiment. Difference in fold change for wild type *CDH1* promoter activity: $P = .001$, for mutant *CDH1* promoter activity: $P = .2$, two-sided Student *t* test. **F**) Expression of EMT-related transcriptional factors zinc finger protein SNAI1, zinc finger protein SNAI2, and twist-related protein TWIST1 in stable MCF7 transfectants was analyzed by immunoblotting. CDH1 = E-cadherin; EMT = epithelial–mesenchymal transition; GAPDH = glyceraldehyde 3-phosphate dehydrogenase; SNAI1 = snail homolog 1; SNAI2 = snail homolog 2; TWIST1 = twist homolog 1.

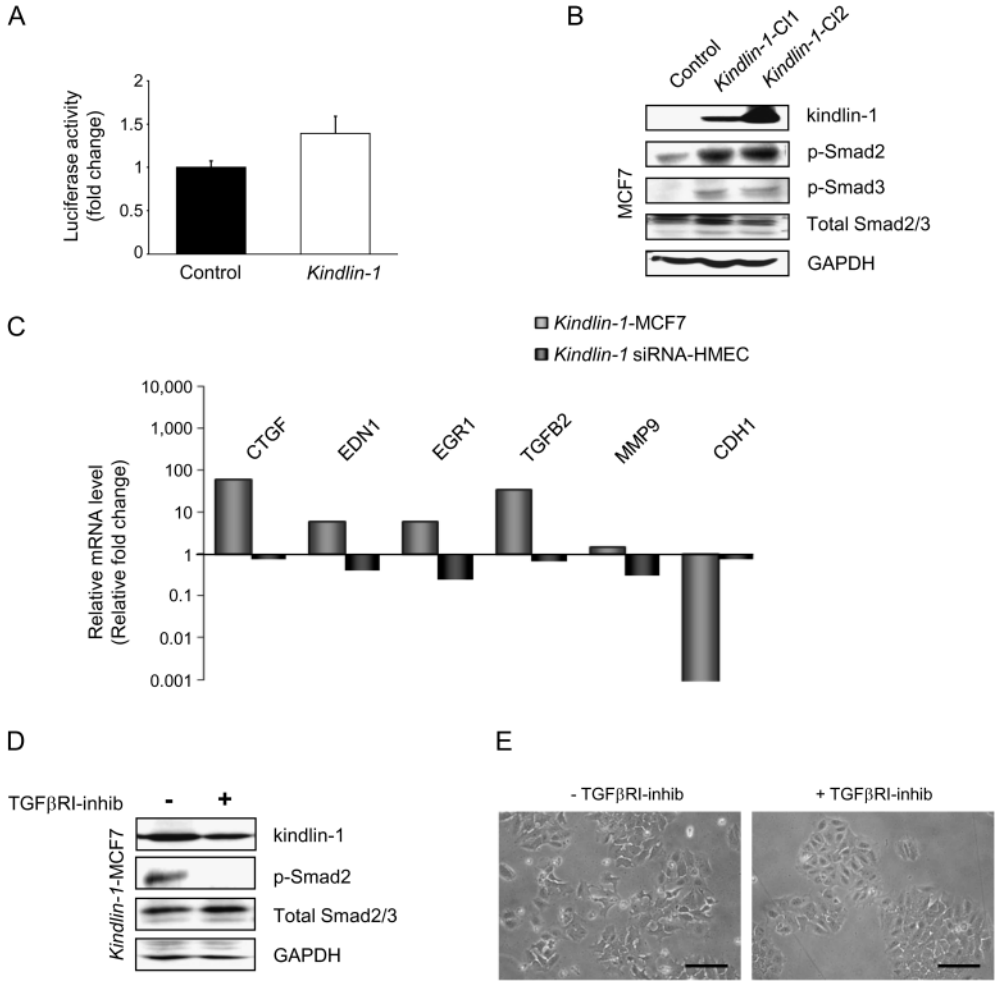

Figure 5. Effect of Kindlin-1 on TGFβ signaling and TGFβ-induced EMT in human mammary cell lines. **A**) MDA-MB-231 cells transfected with the p3TP-lux reporter construct in the presence or absence of *Kindlin-1* were treated for 16 hours with TGFβ1 (2 ng/mL). Luciferase activity was determined and normalized to an internal control. Data are representative of two independent experiments performed in triplicate. Means and upper 95% confidence intervals are shown for triplicates of one experiment. **B**) Expression of total and phosphorylated Smad2 and Smad 3 proteins in control-MCF7 and two clones of *Kindlin-1*-MCF7 cells (*Kindlin-1*-Cl1 and *Kindlin-1*-Cl2). **C**) Expression of TGFβ target genes in *Kindlin-1*-expressing MCF7 cells or *Kindlin-1*-depleted HMECs was evaluated by quantitative real-time polymerase chain reaction. Each **bar** represents expression of a target gene as fold change relative to the controls. Results are representative of one experiment performed for several clones. Differences in fold change are statistically significant: for *CTGF*, $P = .02$; for *EDN1*: $P < .001$; for *EGR1*: $P = .10$; for *TGFβ2*: $P = .004$, for *MMP9*: $P = .003$, Student *t* test. **D**) Expression of phosphorylated Smad2 in MCF7 cells transiently expressing kindlin-1 after treatment for 24 hours with the TGFβR1 inhibitor SB431542 (10 μM). **E**) Morphology of *Kindlin-1*-expressing MCF7 cells untreated or treated with SB431542 was revealed by phase contrast microscopy. Scale bar = 200 μm. CTGF = connective tissue growth factor; EDN1 = endothelin 1; EGR1 = early growth response 1; EMT = epithelial–mesenchymal transition; GAPDH = glyceraldehyde 3-phosphate dehydrogenase; HMEC = human mammary epithelial cells; MMP9 = matrix metallopeptidase 9; TGFβ1 = transforming growth factor β1; Smad2 = SMAD family homolog 2.

endothelin-1 (*EDN1*), *early growth response 1 (EGR1)*, *TGFβ2*, and *matrix metallopeptidase 9* (*MMP9*) was higher in *Kindlin-1* cells and reduced in *Kindlin-1*-depleted cells (relative fold change in mRNA expression, *Kindlin-1*-overexpressing MCF7 cells vs *Kindlin-1*-depleted HMEC cells: *CTGF*, 1.0 vs 57.75, difference = 56.74, 95% CI = 13.92 to 99.57, $P = .02$; *EDN1*, 1.0 vs 5.91, difference = 4.9, 95% CI = 4.25 to 5.56, $P < .001$; *EGR1*, 1.0 vs 5.83, difference = 4.83, 95% CI = −1.95 to 11.59, $P = .10$; *TGFβ2*, 1.0 vs 33.47, difference = 32.47, 95% CI = 19.34 to 45.60, $P = .004$; *MMP9*, 1.0 vs 1.44, difference = 0.44, 95% CI = 0.27 to 0.60, $P = .003$, Figure 5, C).

Finally, we used the specific TGFβR1 kinase inhibitor SB431542 to ascertain whether *Kindlin-1*-induced EMT would require signaling through the TGFβ receptor. This inhibitor prevented the phosphorylation of Smad2 (Figure 5, D) and the TGFβ-induced EMT in *Kindlin-1* cells (Figure 5, E). Together, these data suggest that *Kindlin-1*-induced EMT is TGFβ dependent.

Notably, after exposure to TGFβ, *Kindlin-1*-siRNA–treated HMECs maintained cell–cell adhesion and partially retained their original cobblestone-like epithelial morphology (Figure 6, A, B). In contrast, control cells treated with TGFβ lost their cell–cell contacts and displayed a fibroblast-like morphotype (Figure 6, B). Consistently, the depletion of the E-cadherin and β-catenin epithelial markers induced by TGFβ was suppressed in *Kindlin-1*-silenced cells. Similarly, the induction by TGFβ of the mesenchymal markers vimentin, fibronectin, and α-actin was repressed in *Kindlin-1*-silenced cells (Figure 6, C). These results indicate that

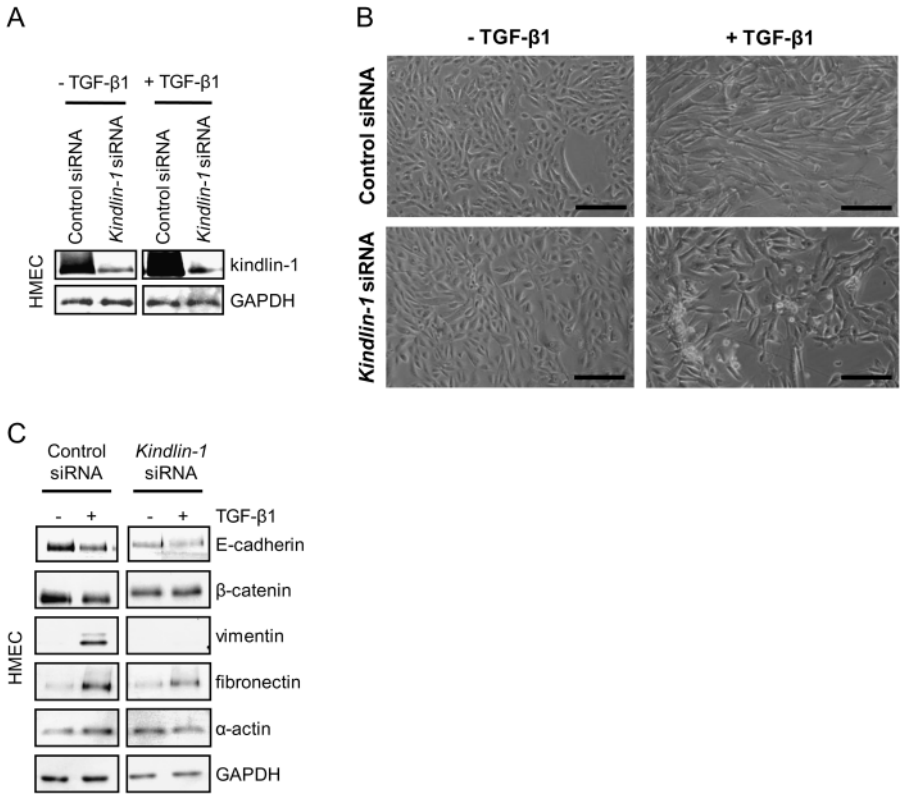

Figure 6. Effect of *Kindlin-1* silencing on the TGFβ-mediated EMT. **A**) Kindlin-1 protein expression in control siRNA-HMECs or *Kindlin-1* siRNA-HMECs untreated or treated for 48 hours with TGFβ1 (5 ng/mL) as determined by immunoblotting. **B**) Morphology of control siRNA-HMECs or *Kindlin-1* siRNA-HMECs untreated or treated with TGFβ1 was revealed by phase contrast microscopy. Scale bar = 200 μm. **C**) Expression of epithelial markers E-cadherin and β-catenin, and mesenchymal markers vimentin, fibronectin, and smooth muscle actin was examined by immunoblotting in control and *Kindlin-1* siRNA-HMECs untreated or treated with TGFβ1. GAPDH = glyceraldehyde 3-phosphate dehydrogenase; HMEC = human mammary epithelial cells; siRNA = short interfering ribonucleic acid; TGFβ1 = transforming growth factor β1.

kindlin-1 suppression restricted the TGFβ-dependent EMT phenotype.

Effect of Kindlin-1 Knockdown on Primary Breast Tumor Growth and Lung Metastasis

To further investigate whether *Kindlin-1* may regulate invasive tumor growth and lung metastasis, we used the highly metastatic 4T1 syngeneic mouse model in which kindlin-1 expression was depleted. The orthotopic injection of *Kindlin-1* shRNA-4T1, or control shRNA-4T1 cells (n = 6 and 10, respectively) into the mammary fat pad of syngeneic BALB/c mice led to the formation of primary mammary tumors in all mice. However, the mean tumor size in *Kindlin-1*-knockdown mice was statistically significantly lower (85% decrease) than in control mice (mean tumor size, *Kindlin-1*-depleted cells vs control cells, 0.36 cm^3 vs 2.46 cm^3, difference = 2.10 cm^3, 95% CI = 1.21 to 2.98, $P < .001$, Figure 7, A and B).

Notably, immunohistochemistry of tumors derived from our mouse model showed that the *Kindlin-1*-silenced tumors exhibited higher E-cadherin levels with more membranous staining than control tumors (Figure 7, C). Taken together, these data suggest that properties of the EMT are manifest in *Kindlin-1*-expressing cells in vivo and are weakened when *Kindlin-1* is silenced.

Finally, we assessed the effect of kindlin-1 depletion on the lung metastatic potential of breast cancer cells (Figure 7, D and E). Although macroscopic metastases were found in lung sections of control mice, no lung micrometastases were detected in *Kindlin-1*-knockdown mice (mean number of metastatic loci in the lungs of *Kindlin-1*-knockdown mice vs control mice, 0 vs 4.60, difference = 4.60, 95% CI = 1.79 to 7.41, $P = .003$, Figure 7, D). These results show that *Kindlin-1* silencing inhibited lung metastasis of 4T1 breast cancer cells.

Discussion

To our knowledge, this is the first study to show that kindlin-1 expression in breast tumors is associated with lung metastasis and lung metastasis–free survival. We provide evidence that kindlin-1 is potentially a clinically relevant mediator of lung metastasis in breast cancer and possibly other carcinomas metastasizing to the lung such as colon cancer, for which overexpression of kindlin-1 was previously reported in a small cohort of patients (seven of 10 patients) (55). In addition, we show that kindlin-1 is overexpressed in lung primary tumors, in which 60-fold increased expression of the gene was previously described (six of 10 lung tumors) (55). Importantly, *Kindlin-1* expression is strongly associated with metastasis-free survival of patients with lung adenocarcinomas.

In addition, our in vitro studies showed that kindlin-1-expressing cells displayed increased proliferation, clonogenicity, and invasion, which are hallmarks of the initiation and progression of primary cancers to metastasis (3,7). Our data are consistent with previous reports on Kindler syndrome keratinocytes and *Kindlin-1*-deficient mice showing decreased proliferation, impaired cell adhesion, and delayed cell spreading (26,56,57). Although a higher propensity to develop cancer has been suggested for Kindler syndrome patients, there is a clear distinction between this inherited disease in which *Kindlin-1* is inactivated and the sporadic cancers reported here in which *Kindlin-1* is wild type and overexpressed. The mechanisms

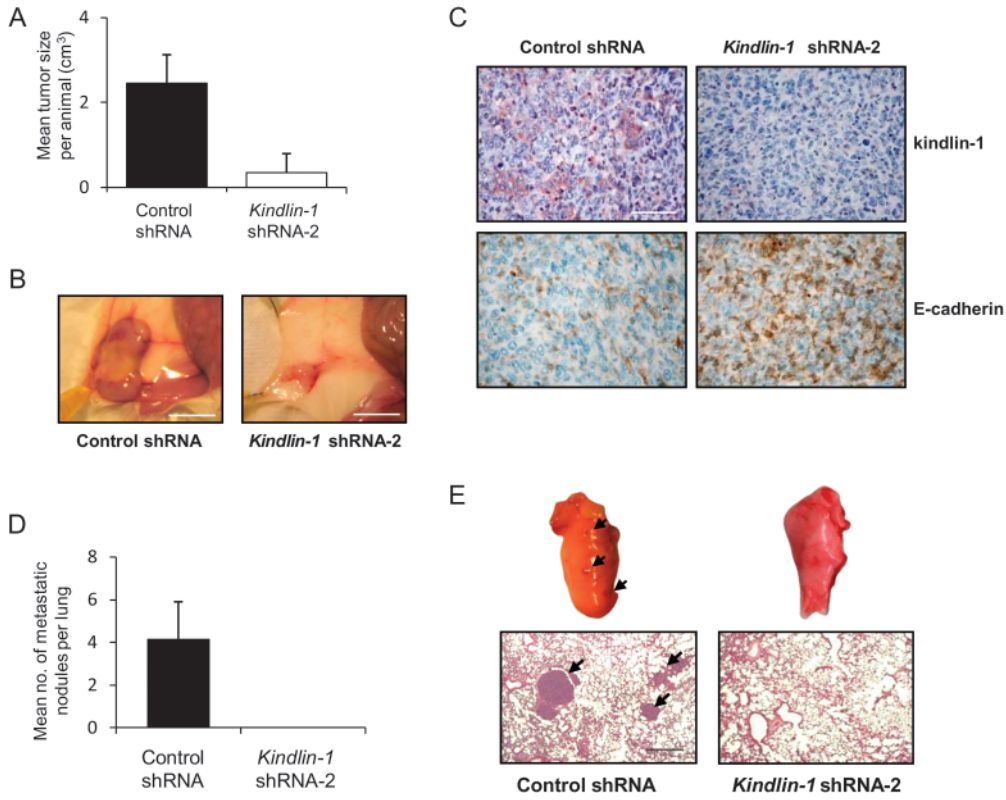

Figure 7. Effect of *Kindlin-1* knockdown on tumorigenic and metastatic potential to lungs in highly invasive 4T1 breast cancer cells. **A**) 4T1 cells transduced with *Kindlin-1* shRNA-2 or control shRNA were injected into the mammary fat pad of syngeneic BALB/c mice (n = 6 and 10, respectively). At 24 days after injection, mean tumor volume was determined in each group of mice; **bars** represent the means and upper 95% confidence intervals; $P < .001$, Student *t* test. **B**) Two representative images of primary tumors from control shRNA and *Kindlin-1* shRNA mice, scale bar = 1 cm. **C**) Primary tumor sections from the *Kindlin-1*-depleted cells were stained for kindlin-1 and E-cadherin. Original magnification ×400, scale bar = 50 μm. **D**) Mean number of lung nodules in control shRNA and *Kindlin-1* shRNA mice (n = 6 and 10, respectively). **Bars** represent the means and upper 95% confidence intervals; $P = .003$, Student *t* test. **E**) Two representative images of lungs harvested from control and *Kindlin-1* shRNA mice (top) and of hematoxylin-stained sections of these lungs (bottom). The **black arrows** indicate metastatic foci. Original magnification ×100, scale bar = 50 μm. shRNA = short hairpin RNA.

underlying skin cancers in Kindler Syndrome are likely to be different from the *Kindlin-1* alterations described here.

Consistent with the role of kindlin-1 in the progression of human cancers, we have shown that *Kindlin-1* silencing prevented tumor growth and lung metastasis in mice using an orthotopic and syngeneic breast tumor model. Although metastasis-associated genes are usually not involved in the growth of primary tumors, kindlin-1, like some other mediators of breast cancer metastasis to the lungs (12,30), may facilitate both breast tumorigenicity and lung metastasis. However, we did not find any association between kindlin-1 expression and breast tumor size in clinical human breast cancer patients. Indeed, a multivariable analysis assessing *Kindlin-1* expression and tumor size in our validation breast tumor dataset (n = 721) showed that *Kindlin-1* was an independent predictor of lung metastasis (not shown).

Kindlin-1 has been shown to be an essential regulator of integrin signaling and cellular adhesion to the ECM proteins such as fibronectin and laminin (22). A recent study (58) demonstrated that β1 integrin signaling is a critical regulator of the proliferation of micrometastatic breast cancer cells in lungs. Furthermore, this process was dependent on the activation of focal adhesion kinase (FAK), which is, like β-integrins, a binding partner of kindlin-1 (59). Thus, the possible implication of the integrin-FAK axis in kindlin-1-mediated lung metastasis is not excluded. Because integrins and adhesion to ECM components may regulate cadherin-dependent cell adhesion mechanisms, kindlin-1 might function at the intersection of multiple signaling pathways and cellular functions during neoplasia.

We have provided evidence that kindlin-1 initiates TGFβ-dependent EMT operating through reduced expression and relocalization of E-cadherin coupled with the induction of several mesenchymal markers such as N-cadherin and fibronectin. Both TGFβ and EMT are potent components of signaling and cellular alterations involved in cancer initiation, invasive growth, and metastasis (60). Most notably, transduced cancer cells expressing kindlin-1 exhibit a constitutive TGFβ-dependent activation of the canonical TGFβ signaling elements Smad-2 and Smad-3 coupled with the transcription of several TGFβ and Smad-inducible genes such as *CTGF*, *EDN1*, and *MMP9*, which are known to be involved in breast cancer progression. In line with our findings, TGFβ has been shown to enhance lung metastasis formation in several transgenic mouse models (61,62). More recently, a TGFβ response gene signature was shown to predict lung metastasis in human breast cancer (53). The authors demonstrated that TGFβ signaling in

the breast tumor microenvironment primes cancer cells for metastasis to the lungs (53).

This study has several potential limitations. First, we were not able to assess the prognostic value of *Kindlin-1* expression in other cancers metastasizing to the lung because of the lack of documented clinical follow-up. In future investigations, it will be important to determine the involvement of *Kindlin-1* in large and well-documented cohorts of colon and bladder cancer patients. Second, our study did not explain in detail the reciprocal crosstalk between kindlin-1 and TGFβ in EMT. Clearly, kindlin-1 may provide a new link between TGFβ, the ECM, and cell–cell adhesion systems in the tumor microenvironment. Although, our results suggest interdependent functions of kindlin-1 and TGFβ in the fine-tuning of EMT and neoplasia, the molecular dissection of this reciprocal crosstalk needs further investigations.

In conclusion, our study suggests that the role of kindlin-1 in human cancers should be assessed further and its possible value for guiding diagnostics and therapeutics considered. First, *Kindlin-1* analysis can be used to identify breast cancer patients with higher risk of developing lung metastasis. Second, targeting kindlin-1 function may be an effective strategy for blocking the EMT and metastasis. Given the importance of the EMT and lung metastasis in the progression of other tumor types, *Kindlin-1* may also have much broader clinical utility relevant to other cancer types.

References

1. Gupta GP, Massague J. Cancer metastasis: building a framework. *Cell.* 2006;127(4):679–695.
2. Fidler IJ. The pathogenesis of cancer metastasis: the 'seed and soil' hypothesis revisited. *Nat Rev Cancer.* 2003;3(6):453–458.
3. Steeg PS. Tumor metastasis: mechanistic insights and clinical challenges. *Nat Med.* 2006;12(8):895–904.
4. Eccles SA, Welch DR. Metastasis: recent discoveries and novel treatment strategies. *Lancet.* 2007;369(9574):1742–1757.
5. Chambers AF, Groom AC, MacDonald IC. Dissemination and growth of cancer cells in metastatic sites. *Nat Rev Cancer.* 2002;2(8):563–572.
6. Chin L, Gray JW. Translating insights from the cancer genome into clinical practice. *Nature.* 2008;452(7187):553–563.
7. Hanahan D, Weinberg RA. The hallmarks of cancer. *Cell.* 2000;100(1):57–70.
8. Kang Y. Functional genomic analysis of cancer metastasis: biologic insights and clinical implications. *Expert Rev Mol Diagn.* 2005;5(3):385–395.
9. Ramaswamy S, Ross KN, Lander ES, Golub TR. A molecular signature of metastasis in primary solid tumors. *Nat Genet.* 2003;33(1):49–54.
10. van 't Veer LJ, Dai H, van de Vijver MJ, et al. Gene expression profiling predicts clinical outcome of breast cancer. *Nature.* 2002;415(6871):530–536.
11. Yang J, Mani SA, Donaher JL, et al. Twist, a master regulator of morphogenesis, plays an essential role in tumor metastasis. *Cell.* 2004;117(7):927–939.
12. Minn AJ, Gupta GP, Siegel PM, et al. Genes that mediate breast cancer metastasis to lung. *Nature.* 2005;436(7050):518–524.
13. Clark EA, Golub TR, Lander ES, Hynes RO. Genomic analysis of metastasis reveals an essential role for RhoC. *Nature.* 2000;406(6795):532–535.
14. Bos PD, Zhang XH, Nadal C, et al. Genes that mediate breast cancer metastasis to the brain. *Nature.* 2009;459(7249):1005–1009.
15. Landemaine T, Jackson A, Bellahcene A, et al. A six-gene signature predicting breast cancer lung metastasis. *Cancer Res.* 2008;68(15):6092–6099.
16. Driouch K, Bonin F, Sin S, Clairac G, Lidereau R. Confounding effects in "a six-gene signature predicting breast cancer lung metastasis": reply. *Cancer Res.* 2009;69(24):9507–9511.
17. Culhane AC, Quackenbush J. Confounding effects in "a six-gene signature predicting breast cancer lung metastasis". *Cancer Res.* 2009;69(18):7480–7485.
18. Siegel DH, Ashton GH, Penagos HG, et al. Loss of kindlin-1, a human homolog of the Caenorhabditis elegans actin-extracellular-matrix linker protein UNC-112, causes Kindler syndrome. *Am J Hum Genet.* 2003;73(1):174–187.
19. Jobard F, Bouadjar B, Caux F, et al. Identification of mutations in a new gene encoding a FERM family protein with a pleckstrin homology domain in Kindler syndrome. *Hum Mol Genet.* 2003;12(8):925–935.
20. Kuijpers TW, van de Vijver E, Weterman MA, et al. LAD-1/variant syndrome is caused by mutations in FERMT3. *Blood.* 2009;113(19):4740–4746.
21. Svensson L, Howarth K, McDowall A, et al. Leukocyte adhesion deficiency-III is caused by mutations in KINDLIN3 affecting integrin activation. *Nat Med.* 2009;15(3):306–312.
22. Ussar S, Moser M, Widmaier M, et al. Loss of Kindlin-1 causes skin atrophy and lethal neonatal intestinal epithelial dysfunction. *PLoS Genet.* 2008;4(12):e1000289.
23. Larjava H, Plow EF, Wu C. Kindlins: essential regulators of integrin signalling and cell-matrix adhesion. *EMBO Rep.* 2008;9(12):1203–1208.
24. Montanez E, Ussar S, Schifferer M, et al. Kindlin-2 controls bidirectional signaling of integrins. *Genes Dev.* 2008;22(10):1325–1330.
25. Kloeker S, Major MB, Calderwood DA, Ginsberg MH, Jones DA, Beckerle MC. The Kindler syndrome protein is regulated by transforming growth factor-beta and involved in integrin-mediated adhesion. *J Biol Chem.* 2004;279(8):6824–6833.
26. Herz C, Aumailley M, Schulte C, Schlotzer-Schrehardt U, Bruckner-Tuderman L, Has C. Kindlin-1 is a phosphoprotein involved in regulation of polarity, proliferation, and motility of epidermal keratinocytes. *J Biol Chem.* 2006;281(47):36082–36090.
27. Zhang XH, Wang Q, Gerald W, et al. Latent bone metastasis in breast cancer tied to Src-dependent survival signals. *Cancer Cell.* 2009;16(1):67–78.
28. Rakha EA, El-Sayed ME, Lee AH, et al. Prognostic significance of Nottingham histologic grade in invasive breast carcinoma. *J Clin Oncol.* 2008;26(19):3153–3158.
29. Minn AJ, Kang Y, Serganova I, et al. Distinct organ-specific metastatic potential of individual breast cancer cells and primary tumors. *J Clin Invest.* 2005;115(1):44–55.
30. Minn AJ, Gupta GP, Padua D, et al. Lung metastasis genes couple breast tumor size and metastatic spread. *Proc Natl Acad Sci U S A.* 2007;104(16):6740–6745.
31. van de Vijver MJ, He YD, van't Veer LJ, et al. A gene-expression signature as a predictor of survival in breast cancer. *N Engl J Med.* 2002;347(25):1999–2009.
32. Wang Y, Klijn JG, Zhang Y, et al. Gene-expression profiles to predict distant metastasis of lymph-node-negative primary breast cancer. *Lancet.* 2005;365(9460):671–679.
33. Desmedt C, Piette F, Loi S, et al. Strong time dependence of the 76-gene prognostic signature for node-negative breast cancer patients in the TRANSBIG multicenter independent validation series. *Clin Cancer Res.* 2007;13(11):3207–3214.
34. Lee ES, Son DS, Kim SH, et al. Prediction of recurrence-free survival in postoperative non-small cell lung cancer patients by using an integrated model of clinical information and gene expression. *Clin Cancer Res.* 2008;14(22):7397–7404.
35. Shedden K, Taylor JM, Enkemann SA, et al. Gene expression-based survival prediction in lung adenocarcinoma: a multi-site, blinded validation study. *Nat Med.* 2008;14(8):822–827.
36. Ross DT, Scherf U, Eisen MB, et al. Systematic variation in gene expression patterns in human cancer cell lines. *Nat Genet.* 2000;24(3):227–235.
37. Aslakson CJ, Miller FR. Selective events in the metastatic process defined by analysis of the sequential dissemination of subpopulations of a mouse mammary tumor. *Cancer Res.* 1992;52(6):1399–1405.
38. Wrana JL, Attisano L, Carcamo J, et al. TGF beta signals through a heteromeric protein-kinase receptor complex. *Cell.* 1992;71(6):1003–1014.
39. Batlle E, Sancho E, Franci C, et al. The transcription factor snail is a repressor of E-cadherin gene expression in epithelial tumour cells. *Nat Cell Biol.* 2000;2(2):84–89.

40. Bieche I, Parfait B, Le Doussal V, et al. Identification of CGA as a novel estrogen receptor-responsive gene in breast cancer: an outstanding candidate marker to predict the response to endocrine therapy. *Cancer Res.* 2001;61(4):1652–1658.
41. De Wever O, Hendrix A, De Boeck A, et al. Modeling and quantification of cancer cell invasion through collagen type I matrices. *Int J Dev Biol.* 2010;54(5):887–896.
42. Sorlie T, Perou CM, Tibshirani R, et al. Gene expression patterns of breast carcinomas distinguish tumor subclasses with clinical implications. *Proc Natl Acad Sci U S A.* 2001;98(19):10869–10874.
43. Sabates-Bellver J, Van der Flier LG, de Palo M, et al. Transcriptome profile of human colorectal adenomas. *Mol Cancer Res.* 2007;5(12):1263–1275.
44. Kaiser S, Park YK, Franklin JL, et al. Transcriptional recapitulation and subversion of embryonic colon development by mouse colon tumor models and human colon cancer. *Genome Biol.* 2007;8(7):R131.
45. Sanchez-Carbayo M, Socci ND, Lozano J, Saint F, Cordon-Cardo C. Defining molecular profiles of poor outcome in patients with invasive bladder cancer using oligonucleotide microarrays. *J Clin Oncol.* 2006;24(5):778–789.
46. Dyrskjot L, Kruhoffer M, Thykjaer T, et al. Gene expression in the urinary bladder: a common carcinoma in situ gene expression signature exists disregarding histopathological classification. *Cancer Res.* 2004;64(11):4040–4048.
47. Wallace TA, Prueitt RL, Yi M, et al. Tumor immunobiological differences in prostate cancer between African-American and European-American men. *Cancer Res.* 2008;68(3):927–936.
48. Liu P, Ramachandran S, Ali Seyed M, et al. Sex-determining region Y box 4 is a transforming oncogene in human prostate cancer cells. *Cancer Res.* 2006;66(8):4011–4019.
49. Landi MT, Dracheva T, Rotunno M, et al. Gene expression signature of cigarette smoking and its role in lung adenocarcinoma development and survival. *PLoS One.* 2008;3(2):e1651.
50. Su LJ, Chang CW, Wu YC, et al. Selection of DDX5 as a novel internal control for Q-RT-PCR from microarray data using a block bootstrap re-sampling scheme. *BMC Genomics.* 2007;8:140–151.
51. Wachi S, Yoneda K, Wu R. Interactome-transcriptome analysis reveals the high centrality of genes differentially expressed in lung cancer tissues. *Bioinformatics.* 2005;21(23):4205–4208.
52. Hendrix ND, Wu R, Kuick R, Schwartz DR, Fearon ER, Cho KR. Fibroblast growth factor 9 has oncogenic activity and is a downstream target of Wnt signaling in ovarian endometrioid adenocarcinomas. *Cancer Res.* 2006;66(3):1354–1362.
53. Padua D, Zhang XH, Wang Q, et al. TGFbeta primes breast tumors for lung metastasis seeding through angiopoietin-like 4. *Cell.* 2008;133(1):66–77.
54. Shipitsin M, Campbell LL, Argani P, et al. Molecular definition of breast tumor heterogeneity. *Cancer Cell.* 2007;11(3):259–273.
55. Weinstein EJ, Bourner M, Head R, Zakeri H, Bauer C, Mazzarella R. URP1: a member of a novel family of PH and FERM domain-containing membrane-associated proteins is significantly over-expressed in lung and colon carcinomas. *Biochim Biophys Acta.* 2003;1637(3):207–216.
56. Has C, Ludwig RJ, Herz C, et al. C-terminally truncated kindlin-1 leads to abnormal adhesion and migration of keratinocytes. *Br J Dermatol.* 2008;159(5):1192–1196.
57. Lai-Cheong JE, Parsons M, Tanaka A, et al. Loss-of-function FERMT1 mutations in kindler syndrome implicate a role for fermitin family homolog-1 in integrin activation. *Am J Pathol.* 2009;175(4):1431–1441.
58. Shibue T, Weinberg RA. Integrin beta1-focal adhesion kinase signaling directs the proliferation of metastatic cancer cells disseminated in the lungs. *Proc Natl Acad Sci U S A.* 2009;106:10290–10295.
59. Has C, Herz C, Zimina E, et al. Kindlin-1 Is required for RhoGTPase-mediated lamellipodia formation in keratinocytes. *Am J Pathol.* 2009;175(4):1442–1452.
60. Thiery JP. Epithelial-mesenchymal transitions in development and pathologies. *Curr Opin Cell Biol.* 2003;15(6):740–746.
61. Muraoka RS, Dumont N, Ritter CA, et al. Blockade of TGF-beta inhibits mammary tumor cell viability, migration, and metastases. *J Clin Invest.* 2002;109(12):1551–1559.
62. Siegel PM, Shu W, Cardiff RD, Muller WJ, Massague J. Transforming growth factor beta signaling impairs Neu-induced mammary tumorigenesis while promoting pulmonary metastasis. *Proc Natl Acad Sci U S A.* 2003;100(14):8430–8435.

Funding

European Commission Framework Program VI MetaBre (CEE LSHC-CT-2004-503049 to S.S., I.B., A.B., V.C., O.d.W., R.L., K.D.); the Breast Cancer Research Foundation (BCRF; to S.S., F.B., I.B., R.L., K.D.); the Region Ile-de-France (I.B., R.L., K.D.); and a grant from the Association Pour la Recherche contre le Cancer (ARC, France; to S.S.).

Notes

S. Sin and F. Bonin contributed equally to this work.

The funders did not have any involvement in the design of the study; the collection, analysis, and interpretation of the data; the writing of the article; or the decision to submit the article for publication.

We thank Aurélie Susini (Oncogénétique,Institut Curie/Hôpital René Huguenin, France) and Catherine Régnier (Anatomopathologie, Institut Curie/Hôpital René Huguenin) for expert technical assistance; Céline Prunier (INSERM U893, Hôpital Saint-Antoine, France) for scientific advice; Marina Glukhova (UMR 144, CNRS-Institut Curie, France) for the contribution in animal experimentation; and all the partners of the METABRE consortium for fruitful discussions: A. Teti (University of L'Aquila, Italy), A. Sierra (IDIBELL, Spain), M. Bracke (Ghent University Hospital, Belgium), R. Buccione (ConsorzioMario NegriSud, Italy), P. Clément-Lacroix (Proskelia, France), P. Clézardin (Institut National de la Santé et de la Recherche Médicale, France), S. Eccles (Institute of Cancer Research, UK), M. Ugorski (Wroclaw University of Environmental and Life Sciences, Poland), and G. van der Pluijm (Leiden University Medical Center, the Netherlands).

Affiliations of authors: Institut Curie, Laboratoire d'Oncogénétique, Hôpital René Huguenin, Saint-Cloud, 92210, France; INSERM, U735, Saint-Cloud, 92210, France (SS, FB, FL, IB, RL, KD): Institut Curie, Compartimentation et dynamique cellulaires, Paris, 75248; CNRS, UMR144, Paris, 75248, France (VP); Laboratoire d'Anatomopathologie, Institut Curie/Hôpital René Huguenin, Saint-Cloud, France (DM); Metastasis Research Laboratory, GIGA-Cancer, University of Liège, Liège, Belgium (AB, VC); Department of Radiotherapy and Experimental Cancer Research, Laboratory of Experimental Cancer Research, Ghent University Hospital, Ghent, Belgium (OdW); INSERM UMR_S938, Centre de Recherche Saint-Antoine, Paris, France (CG).